# Ruthenium-based PACT compounds based on an N,S non-toxic ligand: a delicate balance between photoactivation and thermal stability

Jordi-Amat Cuello-Garibo [a], Catriona C. James [a], Maxime A. Siegler [b], Sylvestre Bonnet [a]*

Email: bonnet@chem.leidenuniv.nl

[a] Leiden Institute of Chemistry, Universiteit Leiden, Einsteinweg 55 2333 CC, Leiden, Netherlands
[b] Small Molecule X-ray Crystallography Facility, Johns Hopkins University, 3400N, Charles St, Baltimore, MD, 21218, USA.

**Abstract**: In photoactivated chemotherapy, the photocleavable protecting group that prevents the bioactive compound from interacting with biomolecules in the dark is sometimes cytotoxic, which makes interpretation of phototoxicity challenging. For ruthenium polypyridyl complexes new, non-toxic protecting ligands that prevent a toxic metal complex from binding to biomolecules in the dark, but that can be efficiently photosubstituted upon visible light irradiation to recover the high toxicity of the metal complex, are necessary. In this work, we report on the synthesis, stereochemical characterization and cytotoxicity of a series of polypyridyl complexes; $[Ru(bpy)_2(mtpa)](PF_6)_2$ ([**1**]$(PF_6)_2$, bpy = 2,2'-bipyridine), $[Ru(bpy)(dmbpy)(mtpa)](PF_6)_2$ ([**2**]$(PF_6)_2$, dmbpy = 6,6'-dimethyl-2,2'-bipyridine), and $[Ru(dmbpy)_2(mtpa)](PF_6)_2$ ([**3**]$(PF_6)_2$) based on the non-toxic 3-(methylthio)propylamine protecting ligand (mtpa). The number of methyl groups had a crucial effect on the photochemistry and cytotoxicity of these complexes. The non-strained complex $[\mathbf{1}]^{2+}$ was not capable of fully releasing mtpa and was not phototoxic in lung cancer cells (A549). In the most strained complex $[\mathbf{3}]^{2+}$, thermal stability was lost, leading to poor photoactivation *in vitro* and a generally high toxicity also without light activation. The heteroleptic complex $[\mathbf{2}]^{2+}$ with intermediate strain showed, upon blue light irradiation, efficient mtpa photosubstitution and increased cytotoxicity in cancer cells, but photosubstitution was not selective. Overall, fine-tuning of the lipophilicity and steric strain of ruthenium complexes appears as an efficient method to obtain phototoxic ruthenium-based photoactivated chemotherapeutic prodrugs, at the cost of synthetic simplicity and photosubstitution selectivity.

**Keywords**: photoactivated chemotherapy; metallodrugs; cancer; phototherapy; steric strain; thioether; polypyridyl; photodynamic therapy; photopharmacology.

## I. Introduction

In the last decade, Photoactivated Chemotherapy (PACT) with ruthenium-based complexes has caught attention because it has the potential to control the cytotoxicity of anticancer drugs in space and time. Whereas in Photodynamic Therapy (PDT) cytotoxicity is obtained by the photochemical generation of reactive oxygen species (ROS) such as singlet oxygen [1, 2, 3], in metal-based PACT a new cytotoxic drug is formed *in situ* via photosubstitution of at least one of the ligands of the original pro-drug [4, 5]. In many reported examples, ruthenium PACT agents are based on complexes of the $[Ru(bpy)_2(dmbpy)]^{2+}$ family, where bpy is 2,2'-bipyridine and dmbpy is the sterically hindering ligand 6,6'-dimethyl-2,2'-bipyridine, which increases the distortion of the coordination octahedron [6, 7]. In such strained complexes, the triplet metal-centered excited state ($^3$MC) of the ruthenium complex is lowered

doi: 10.28954/2017.csq.12.002

and can thus be thermally populated from the photochemically generated triplet metal-to-ligand charge-transfer state ($^3$MLCT), leading to photosubstitution of dmbpy by two solvent molecules.
The increased cytotoxicity of the compound by light irradiation was generally attributed to the formation of the bis-aqua complex *cis*-$[Ru(bpy)_2(OH_2)_2]^{2+}$, which may interact with nuclear DNA by analogy with the mode-of-action of cisplatin. However, we and others demonstrated recently that the second photoproduct obtained upon irradiation of $[Ru(bpy)_2(dmbpy)]^{2+}$ in water, *i.e.* the free dmbpy ligand, is the actual cytotoxic species [8, 9]. These findings resulted in the formulation of two questions: first, can we design a light-activated ruthenium complex in which the ruthenium bis-aqua photoproduct is the sole cytotoxic species? And second, if sterically hindering bipyridyl chelates such as dmbpy cannot be used on account of their cytotoxicity, which non-toxic ligands can we use to protect cytotoxic ruthenium aqua complexes, and how can we fine-tune the metal complex to obtain efficient and selective photosubstitution *in vitro*?.
Our group actively investigates the use of thioether ligands for the caging of aquated ruthenium complexes [10]. Thioethers are excellent ligands for ruthenium(II) due to their softness, which often leads to thermally stable complexes. In addition, many ruthenium complexes coordinated to thioethers show selective photosubstitution of the thioether ligand because these types of ligands become more weakly bound in the excited states than nitrogen-based ligands [11, 12]. $[Ru(bpy)_2(mtmp)]Cl_2$ and $[Ru(Ph_2phen)_2(mtmp)]Cl_2$ ($Ph_2phen$ = 4,7-diphenyl-1,10-phenantroline and mtmp = 2-methylthiomethyl pyridine), for example, efficiently photosubstitute the non-toxic N,S ligand mtmp in water [8]. In A549 cancer cells, the former hardly entered the cell because of its too high hydrophilicity, while the latter already showed a strong cytotoxicity in the dark due to its high lipophilicity. Overall, fine-tuning the lipophilicity of these types of compounds seemed necessary to study whether better phototoxicity can be obtained with compounds which penetrate cancer cells in the dark, but that do not activate without irradiation. In the present study, we systematically varied the number of bpy and dmbpy ligands in a series of ruthenium complexes also bearing a 3-(methylthio)propylamine chelating ligand (mtpa). The complexes $[Ru(bpy)_2(mtpa)](PF_6)_2$ ([**1**]$(PF_6)_2$), $[Ru(bpy)(dmbpy)(mtpa)](PF_6)_2$ ([**2a**]$(PF_6)_2$ and [**2b**]$(PF_6)_2$), and $[Ru(dmbpy)_2(mtpa)](PF_6)_2$ ([**3**]$(PF_6)_2$), were prepared (**Figure 1**), their stereochemistry fully characterized, and their cytotoxicity in the dark and under light irradiation evaluated. The effect of the number of methyl groups on the photochemistry, lipophilicity, and cytotoxicity of these complexes is discussed.

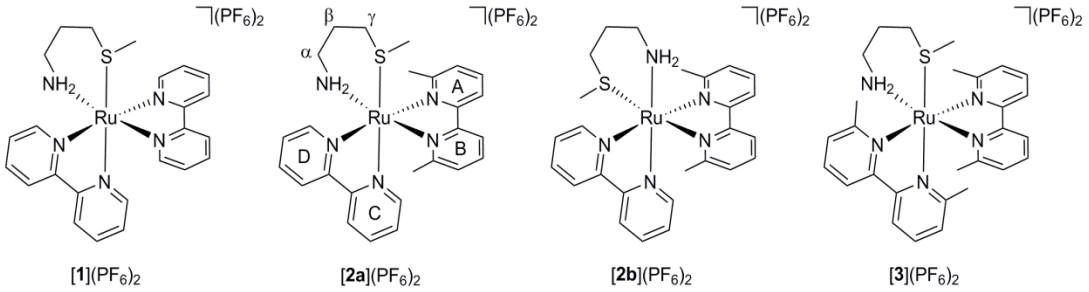


**Figure 1**. Structures of the complexes [**1**]$(PF_6)_2$, [**2a**]$(PF_6)_2$, [**2b**]$(PF_6)_2$, and [**3**]$(PF_6)_2$. The configuration of the sulfur center is not specified. For clarity only the Λ isomers are shown, but all samples were obtained as racemic Δ/Λ mixtures.

## II. Results and Discussion

### Synthesis

Complexes [**1**]$(PF_6)_2$ and [**3**]$(PF_6)_2$ were obtained in a similar manner by reacting their known precursors $[Ru(bpy)_2Cl_2]$ and $[Ru(dmbpy)_2Cl_2]$, respectively, with the mtpa ligand, to afford racemic mixtures. The stereochemistry of these complexes is challenging to establish. Besides the chirality of the octahedron (Δ or Λ), two other sources of isomerism are present for such complexes (**Scheme 1**): the configuration (*S* or *R*) of the sulfur atom, and the chair inversion of the six-membered ring resulting from the coordination of the N,S chelating ligand to the ruthenium centre, which transforms an axial thioether methyl group (*ax*) into an equatorial one (*eq*) and *vice versa*, but without changing the configuration of the sulfur atom. This isomerism leads to a total of four possible isomers, *i.e.* Λ-(*R*)-*eq*-[**Ru**]$^{2+}$,

Λ-(*R*)-*ax*-[**Ru**]$^{2+}$, Λ-(*S*)-*eq*-[**Ru**]$^{2+}$, and Λ-(*S*)-*ax*-[**Ru**]$^{2+}$ (where [**Ru**]$^{2+}$ is either [**1**]$^{2+}$, [**2a**]$^{2+}$, [**2b**]$^{2+}$, or [**3**]$^{2+}$), together with their enantiomers Δ-(*S*)-*eq*-[**Ru**]$^{2+}$, Δ-(*S*)-*ax*-[**Ru**]$^{2+}$, Δ-(*R*)-*eq*-[**Ru**]$^{2+}$, and Δ-(*R*)-*ax*-[**Ru**]$^{2+}$, respectively. According to the signals of $^1$H NMR, complexes [**1**](PF$_6$)$_2$ and [**3**](PF$_6$)$_2$ were obtained as a mixture of two diastereoisomers in 1:0.05 and 1:0.12 ratios, respectively. For the tris-heteroleptic complex [**2**](PF$_6$)$_2$, which bears three different bidentate ligands, a previously reported synthetic route was used [13], which consisted first in preparing *cis*-[Ru(bpy)(dmbpy)(CH$_3$CN)$_2$](PF$_6$)$_2$ ([**4**](PF$_6$)$_2$) by visible light irradiation of the precursor [Ru(bpy)(dmbpy)$_2$](PF$_6$)$_2$ [**5**](PF$_6$)$_2$ in CH$_3$CN, and then reacting [**4**](PF$_6$)$_2$ with mtpa in water. The $^1$H NMR spectrum of the crude product [**2**](PF$_6$)$_2$ showed two doublets at 9.55 and 9.17 ppm, characteristic for the hydrogen in position 6 or 6' on the bpy, in a ratio of 1:0.55. Mass spectrometry showed peaks at m/z = 273.2, 287.4, and 692.0, which corresponds to [Ru(bpy)(dmbpy)(mtpa)]$^{2+}$ (calcd m/z = 273.6), [Ru(dmbpy)$_2$(mtpa)]$^{2+}$ (calcd m/z = 287.6), and {[Ru(bpy)(dmbpy)(mtpa)](PF$_6$)}$^+$ (calcd m/z = 692.1), respectively, indicating the occurrence of ligand scrambling. Since the two doublets in the 9−10 ppm range cannot belong to [Ru(dmbpy)$_2$(mtpa)]$^{2+}$, the two main species present in the mixture share the same mass peaks, *i.e.* they are two of the expected isomers of [**2**]$^{2+}$. Resolution of both isomers by alumina column chromatography using a mixture of DCM/CH$_3$OH (99:1) as eluent did produce a main fraction containing both isomers in a ratio 1:0.07 according to $^1$H NMR.

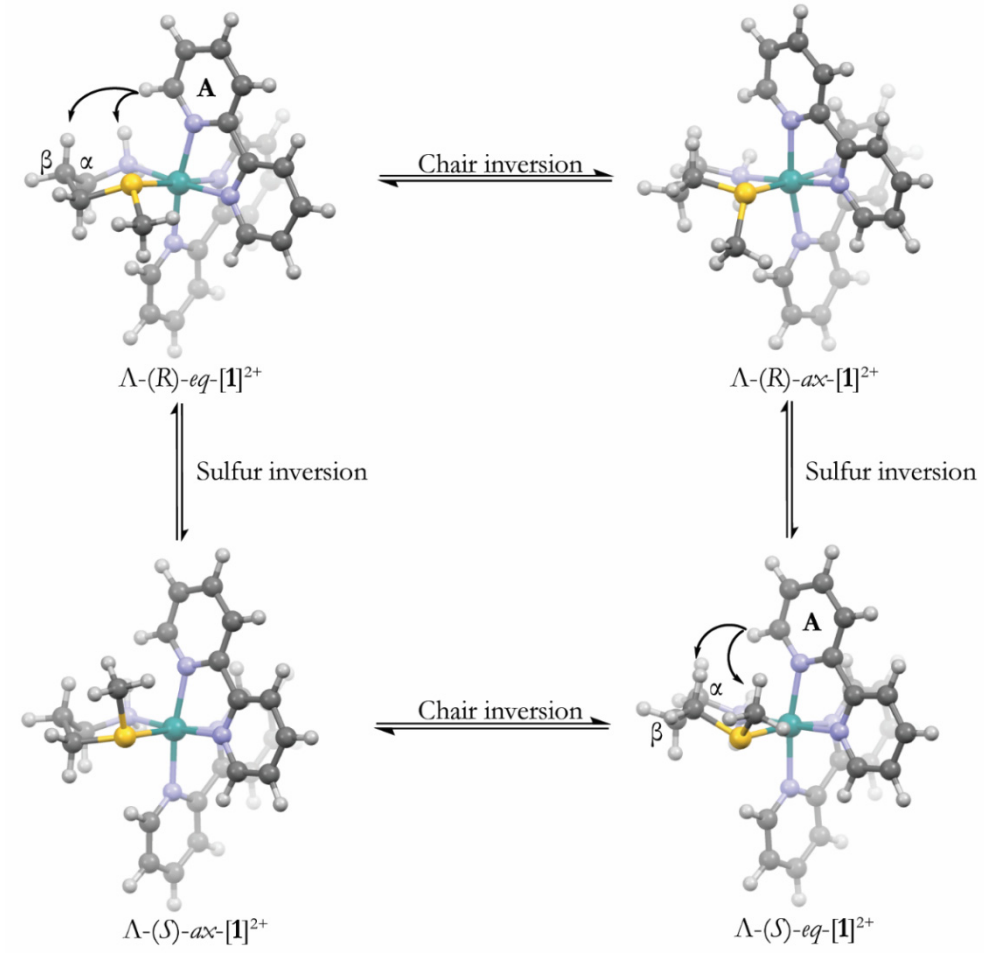


**Scheme 1**. Isomers of [**1**]$^{2+}$ as a result of the inversion of either the chirality of the sulfur atom (R or S) or the conformation of the chair. Isomers Λ-(R)-*eq*-[**1**]$^{2+}$ and Λ-(S)-*eq*-[**1**]$^{2+}$ show distances between $N_{eq}$ and A6 of 3.398 and 2.585 Å, respectively, and distances between the $\alpha_{ax}$ and A6 of 4.638 and 1.983 Å, respectively.

The tris-heteroleptic complex [**2**](PF$_6$)$_2$ bears three different bidentate ligands, so that the two different orientations of mtpa lead to two different regioisomers: either (OC-6-43)-[Ru(bpy)(dmbpy)(mtpa)]$^{2+}$,

in which the thioether sulfur donor is *trans* to the bpy, or (OC-6-34)-[Ru(bpy)(dmbpy)(mtpa)]$^{2+}$, in which the thioether ligand is *trans* to the dmbpy ligand. For simplicity, these two regioisomers are called [**2a**]$(PF_6)_2$ and [**2b**]$(PF_6)_2$, respectively (**Figure 1**). Like for [**1**]$(PF_6)_2$ and [**3**]$(PF_6)_2$, each of the regioisomers of [**2**]$(PF_6)_2$ has four possible isomers, which leads to a total of eight possible Λ diastereoisomers and their corresponding eight Δ enantiomers.
NOESY analysis in $D_2O$ showed an off-diagonal correlation between a proton of the amine and the methyl substituent on the dmbpy for the major isomer, which means that in this isomer the amine must be *trans* to dmbpy. Thus, the major isomer in this fraction was [**2a**]$^{2+}$, while the minor isomer remains unassigned. However, after storage for two weeks as a powder in the freezer (−20 °C), this purified sample had isomerized back into a 1:0.4 mixture of isomers, which showed that isomerization was occurring even in such conditions, and thus that the two isomers cannot be kept in separate flasks. Below, [**2**]$(PF_6)_2$ is used as a mixture of these two regioisomers.

## Characterization by DFT and NOESY studies

In order to understand the stereoselectivity of sulfur coordination in solution, Density Functional Theory (DFT) calculations of complexes [**1**]$^{2+}$, [**2a**]$^{2+}$, [**2b**]$^{2+}$, and [**3**]$^{2+}$ were performed in water using the COSMO model for simulating solvent effects (see Experimental Section). The sulfur atom was either in *R* or *S* configuration, with the methyl group either in equatorial or in axial position of the six-membered ring by inversion of the chair (**Scheme 1**), resulting in a total of four possible isomers per complex. The optimized structures and their energies are given in **Scheme 1**, **Figure S14**, **Figure S15,** and **Table S2**, respectively. Λ-(*S*)-*eq*-[**1**]$^{2+}$ was the lowest in energy, followed by Λ-(*S*)-*ax*-[**1**]$^{2+}$ at +5.4 kJ·mol$^{-1}$, which is obtained by inversion of the chair. NOESY analysis of [**1**]$^{2+}$ in $D_2O$ showed an off-diagonal correlation between the A6 proton on bpy and the $N_{eq}$ proton of mtpa, and a correlation between A6 and the $\alpha_{ax}$ proton (**Figure S4**). In the calculated structure of Λ-(*S*)-*eq*-[**1**]$^{2+}$ the corresponding distances are short, *i.e.* 2.585 and 1.983 Å, respectively (**Scheme 1**). Thus, altogether the DFT and NMR studies suggest that [**1**]$^{2+}$ is a racemic mixture containing Λ-(*S*)-*eq*-[**1**]$^{2+}$ and Δ-(*R*)-*eq*-[**1**]$^{2+}$, which is also the most thermodynamically stable pair of enantiomers.

For the tris-heteroleptic complex [**2**]$^{2+}$, Λ-(*R*)-*eq*-[**2a**]$^{2+}$ appeared to be the most stable in water according to DFT. The isomers of [**2b**]$^{2+}$ were found at higher energies, ranging from +7.5 to +26.6 kJ·mol$^{-1}$. Furthermore, NOESY analysis in $CD_3OD$ showed an off-diagonal correlation between the D6 proton on the bpy of the major isomer with both MeS- and the γ proton of mtpa (**Figure S5**). In the calculated structure of Λ-(*R*)-*eq*-[**2a**]$^{2+}$ the distances between those atoms are short (2.083 and 2.147 Å, respectively, see **Figure 2**), whereas in Λ-(*S*)-*eq*-[**2a**]$^{2+}$ they are much larger, *i.e.* 4.198 and 3.918 Å, respectively. Thus, NMR data agree with DFT that the major and most stable isomer is Λ-(*R*)-*eq*-[**2a**]$^{2+}$.

Finally, for the most strained complex of the series [**3**]$^{2+}$, isomer Λ-(*S*)-*ax*-[**3**]$^{2+}$ was the most stable according to DFT. NOESY analysis in $CD_3OD$ showed an off-diagonal correlation between the methyl substituent DMe and the proton $\gamma_{ax}$, and another correlation between the methyl substituent AMe and the methylthioether group, with a relative intensity of the signals of 65% and 35%, respectively (**Figure S6**). According to the calculated structures, the distances between those hydrogens are 3.439 and 3.102 Å in Λ-(*S*)-*eq*-[**3**]$^{2+}$, 2.133 and 6.246 Å in Λ-(*R*)-*eq*-[**3**]$^{2+}$, and 2.127 and 2.995 Å in Λ-(*S*)-*ax*-[**3**]$^{2+}$, respectively (**Figure 2**). Thus, isomer Λ-(*S*)-*ax*-[**3**]$^{2+}$ fits best with the NOESY data in solution. Overall, irrespective of steric hindrance the major isomer in solution was also the most thermodynamically stable isomer.

To quantify steric hindrance the structural distortion parameter, *i.e.* the bond angle variance ($\sigma^2$), was calculated from the DFT models (**Table S1**) [14, 15]. In a simple assumption, molecules with more methyl groups should have a more distorted coordination sphere, thus a higher $\sigma^2$ value. However, the change in the configuration of the sulfur atom appeared to have a great impact on $\sigma^2$. All isomers with *R* configuration had a higher $\sigma^2$ value than their *S* isomer (e.g. $\sigma^2$ is 62.4 and 45.0 for Λ-(*R*)-*eq*-[**1**]$^{2+}$ and Λ-(*S*)-*eq*-[**1**]$^{2+}$, respectively). The $\sigma^2$ value for the tris-heteroleptic *R* complex Λ-(*R*)-*eq*-[**2a**]$^{+}$ is even higher than that of the, in principle, more strained *S* complex Λ-(*S*)-*eq*-[**3**]$^{+}$ (81.8 *vs.* 76.3). Thus, the orientation

of specific bulky moieties such as $CH_3S$- has a greater effect on the distortion of the octahedron than the number of methyl groups.

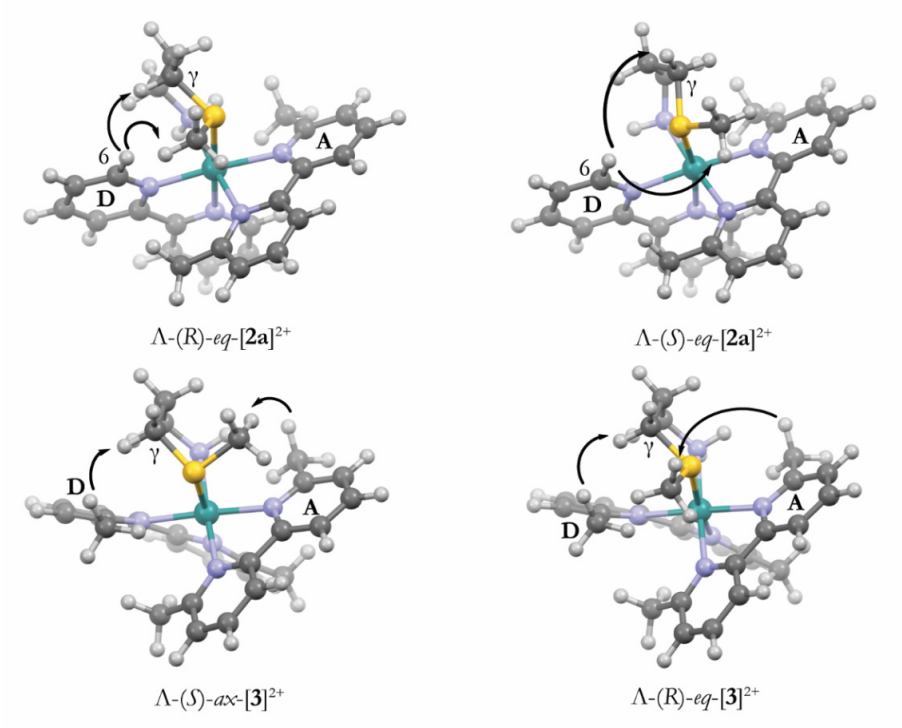


**Figure 2**. Structures of selected isomers of $[\mathbf{2}]^{2+}$ and $[\mathbf{3}]^{2+}$ optimized by DFT in water (COSMO). Isomers Λ-(R)-*eq*-$[\mathbf{2a}]^{2+}$ and Λ-(*S*)-*eq*-$[\mathbf{2a}]^{2+}$ show distances between $\gamma_{ax}$ and D6 of 2.147 and 3.918 Å, respectively, and distances between the methyl thioether group and D6 of 2.083 and 4.198 Å, respectively. Isomers Λ-(*S*)-*ax*-$[\mathbf{3}]^{2+}$ and Λ-(*R*)-*eq*-$[\mathbf{3}]^{2+}$ show distances between $\gamma_{ax}$ and DMe of 2.127 and 2.133 Å, respectively, and distances between the methyl thioether group and AMe of 2.995 and 6.246 Å.

Furthermore, a direct relation between $\sigma^2$ and DFT-calculated energies in water was found only for the non-strained complex $[\mathbf{1}]^{2+}$, for which the least distorted isomer Λ-(*S*)-$[\mathbf{1}]^{2+}$ had the lowest energy. For $[\mathbf{2}]^{2+}$, the most distorted isomer (Λ-(*R*)-*eq*-$[\mathbf{2a}]^{2+}$) had the lowest energy, whereas the $[\mathbf{3}]^{2+}$ isomers Λ-(*S*)-*ax*-$[\mathbf{3}]^{2+}$ and Λ-(*S*)-*eq*-$[\mathbf{3}]^{2+}$, having similar $\sigma^2$ values (76.0 and 76.3, respectively), showed the greatest difference in energy (37.3 kJ·mol$^{-1}$). Since a correlation between octahedral distortion and stability could not be drawn, the inter-ligand repulsion between the methyl substituents and mtpa was also considered. We found that all the isomers that have the $H_{ax}$ in positions 3 and 5 of the six-membered chair facing directly the 6-methyl substituent of dmbpy were always higher in energy. As shown in **Figure 3**, for Λ-(*S*)-*eq*-$[\mathbf{3}]^{2+}$, which is the least stable of the isomers of $[\mathbf{3}]^{2+}$ in water, the distances between $H_{ax}$ in positions 3 and 5 and their spatially closest methyl substituents are only 2.097 and 1.860 Å, respectively. Overall, two factors influence the stability of these complexes and the stereoselectivity of the coordination of mtpa: octahedral distortion and inter-ligand repulsion. In the case of the non-strained complex $[\mathbf{1}]^{2+}$, only the octahedral distortion plays a role, whereas when hindering methyl substituents are introduced in the complex, inter-ligand repulsion becomes the driving force for the diastereoselectivity of the reaction.

## X-Ray crystallography

Single crystals suitable for X-Ray structure determination were obtained for complexes $[\mathbf{1}](PF_6)_2$, $[\mathbf{2a}](PF_6)_2$, and $[\mathbf{3}](PF_6)_2$ by slow vapor diffusion of the solvent of a methanol solution of the complex into

toluene, ethyl acetate, and di-*tert*-butyl ether, respectively. In all structures, the six-membered ring resulting from the coordination of mtpa to the Ru center was found in a chair conformation, as modelled by DFT.

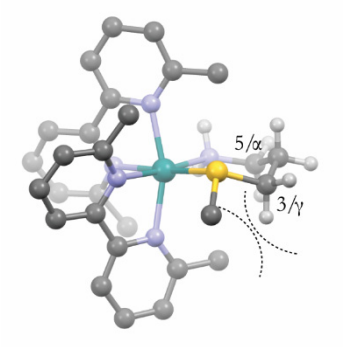


**Figure 3**. Schematic drawing of isomer Λ-(*S*)-*eq*-[**3**]$^{2+}$ showing the steric effect between the methyl substituent on dmbpy facing directly the $H_{ax}$ in positions 3 and 5 of the 6-membered ring in a chair conformation.

For complex [**1**]$(PF_6)_2$ the structure contained the two enantiomers Λ-(*S*) and Δ-(*R*) of $[Ru(bpy)_2(mtpa\text{-}\kappa N,\kappa S)](PF_6)_2 \cdot CH_3OH$. The molecular structure (**Figure 4a**) shows a methyl group in equatorial position, thus being Λ-(*S*)-*eq*-[**1**]$(PF_6)_2$, as suggested by NMR and DFT. Although [**2**]$(PF_6)_2$ was crystallized using a mixture of two regioisomers, the crystal structure contained a racemate of a single isomer of [**2a**]$(PF_6)_2$ containing both configurations Λ-(*R*) and Δ-(*S*). The molecular structure (**Figure 4b**) shows a longer Ru-S bond (2.3668(7) Å) compared to Λ-(*S*)-*eq*-[**1**]$^{2+}$ (2.3314(7) Å, **Table 1**) and the mtpa amine is located *trans* to the dmbpy ligand, confirming the NMR assignment. The methyl group was found in equatorial position, thus the crystallized isomer was Λ-(*R*)-*eq*-[**2a**]$(PF_6)_2$, *i.e.* the isomer suggested also by NMR and DFT. Finally, [**3**]$(PF_6)_2$ contained Λ-(*S*) and Δ-(*R*), and the methylthioether group was axial, fitting NMR and DFT data. The structure shown in **Figure 4c** shows the longest Ru-S bond (2.3845(8) Å) of the series. Thus, more methyl groups in the complex lead, as expected, to longer Ru-S bonds.
The overall agreement between X-ray data, NMR in solution, and DFT, was excellent, and allowed for determining the geometry of these complexes with a great precision.

## Photochemistry and thermal stability

The photoreactivity and thermal stability of all the complexes were studied in water and monitored with a variety of techniques including $^1$H NMR, UV-Vis spectroscopy, and mass spectrometry. Complex [**1**]$(PF_6)_2$, when irradiated with blue light (445 nm), showed a bathochromic shift in the MLCT band with a change in the maximum absorption from 450 to 486 nm, and clear isosbestic points at 325, 390, and 460 nm, indicating a one-step process (**Figure 5a**). After six minutes at ~$3 \cdot 10^{-8}$ mol·s$^{-1}$ photon flux the photoreaction had reached the steady state. Mass spectrometry performed at that point showed major peaks at m/z = 260.0, 269.0, and 536.2, corresponding to $[Ru(bpy)_2(mtpa)]^{2+}$ (calcd m/z = 259.6), $[Ru(bpy)_2(mtpa)(OH_2)]^{2+}$ (calcd m/z = 268.6), and $[Ru(bpy)_2(mtpa)(OH)]^{+}$ (calcd m/z = 536.1) respectively, but no peaks corresponding to the bis photosubstituted species $[Ru(bpy)_2(OH_2)_2]^{2+}$ (calcd m/z = 225.03, **Figure S9**). Thus, only one coordination position was substituted by a water molecule and it appeared impossible to reach full ejection of the bidentate ligand, since peaks belonging to the starting compound [**1**]$^{2+}$ were still present at the steady state. As shown in **Figure 6b**, when this photoreaction was monitored by $^1$H NMR in $D_2O$, doublets at 9.79 and 9.24 ppm, characteristic of the $H_6$ and $H_{6'}$ of bpy in [**1**]$^{2+}$, decreased in intensity after 40 min, whereas new doublets at 9.23 and 9.21 ppm arose for the photoproduct, reaching the steady state with a ratio of 3.4:1 between the photoproduct and the starting complex. Furthermore, the singlet peak of the methyl thioether shifted downfield from 1.20 to 1.92 ppm, which is characteristic for a free methyl thioether. Thus, as shown in **Scheme 2**, the sulfur moiety was photosubstituted, but the amine ligand stayed bound, *i.e.*, the photoproduct

is $[Ru(bpy)_2(mtpa\text{-}\kappa N)(OH_2)]^{2+}$. Furthermore, when the photoproduct was kept in the dark at room temperature, the reverse reaction took place very slowly, with the doublets at 9.23 and 9.21 ppm, characteristics of [**1**](PF$_6$)$_2$, increasing again after 30 days (**Figure 6b**).

**Table 1**. Selected bond lengths (Å) and angles (°) in the crystal structures of Λ-(*S*)-*eq*-[**1**](PF$_6$)$_2$, Λ-(*R*)-*eq*-[**2a**](PF$_6$)$_2$, and Λ-(*S*)-*ax*-[**3**](PF$_6$)$_2$.

| | **Λ-(*S*)-*eq*-[1](PF$_6$)$_2$** | **Λ-(*R*)-*eq*-[2a](PF$_6$)$_2$** | **Λ-(*S*)-a*x*-[3](PF$_6$)$_2$** |
|---|---|---|---|
| **Ru1-S1** | 2.3314(7) | 2.3668(7) | 2.3845(8) |
| **Ru1-N1** | 2.079(2) | 2.117(2) | 2.102(2) |
| **Ru1-N2** | 2.066(2) | 2.112(2) | 2.113(2) |
| **Ru1-N3** | 2.079(2) | 2.064(2) | 2.087(2) |
| **Ru1-N4** | 2.083(2) | 2.081(2) | 2.087(2) |
| **Ru1-N5** | 2.149(2) | 2.167(2) | 2.164(2) |
| **N5-C21-C23-S1** | 12.8(2) | - | - |
| **N5-C26-C24-S1** | - | 8.1(2) | - |
| **N5-C27-C25-S1** | - | - | 4.7(2) |

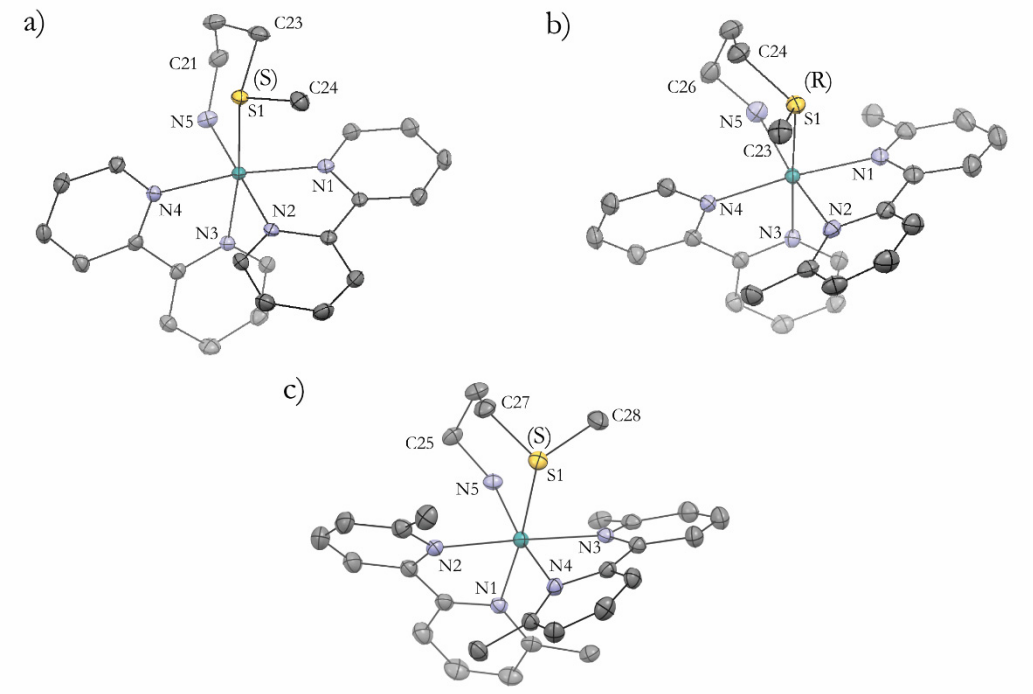


**Figure 4**. Projection of the cationic complex in the crystal structure of the Λ enantiomer of a) Λ-(*S*)-*eq*-[**1**](PF$_6$)$_2$, b) Λ-(*R*)-*eq*-[**2a**](PF$_6$)$_2$, and c) Λ-(*S*)-*ax*-[**3**](PF$_6$)$_2$. Hexafluoridophosphate counteranions, hydrogen atoms, lattice $CH_3OH$ (for [**1**](PF$_6$)$_2$), and disorder have been omitted for clarity.

The reversibility of the ring opening photoreaction was also studied using UV-Vis spectroscopy by irradiating [**1**](PF$_6$)$_2$ four times during 5 min, each time followed by ~2 h of equilibration in the dark at 37 °C (to increase the rate of back coordination). As shown in **Figure 6a**, the ring opening is clearly reversible. Photosubstitution of only one monodentate amine or pyridine ligand L in ruthenium [Ru(bpy)$_2$(L)$_2$]$^{2+}$ complexes is classical in the literature [16, 17], as well as hemilability followed by either fast rechelation (also called recaptation) or full dissociation of the bidentate ligand [18, 19, 20]. However, hemilability followed by such a slow rechelation is rare. Here it appears to be a consequence of the difference in binding properties between the thioether and amine donor atoms. Thus, complex [**1**]$^{2+}$ shows a light-controlled Ru-S bond breaking and thermal recovery, *i.e.*, it behaves like a photoswitch (**Scheme 2**).

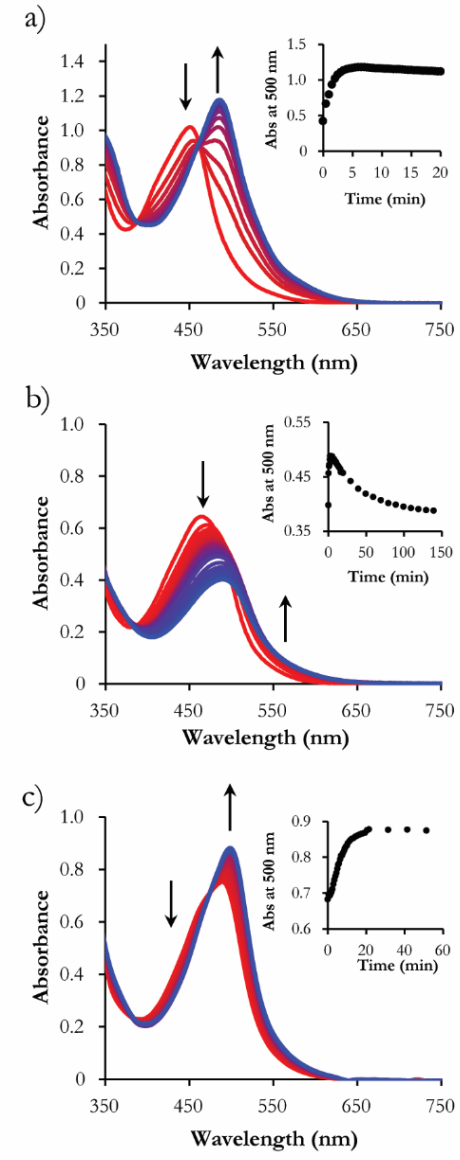


**Figure 5**. Evolution of the UV-Vis spectra of water solutions of (a) [**1**](PF$_6$)$_2$ (0.145 mM), (b) [**2**](PF$_6$)$_2$ (0.101 mM), (c) [**3**](PF$_6$)$_2$ (0.123 mM) upon irradiation with a 445 nm LED (2.9 ± 0.1·10$^{-8}$ mol·s$^{-1}$) under N$_2$ at 25 °C. Insets: evolution of the absorbance at 500 nm *vs.* time.

The photoreactivity of the most strained complex $[\mathbf{3}]^{2+}$ was studied in water for comparison. First, $[\mathbf{3}](PF_6)_2$ was converted to the chloride salt $[\mathbf{3}]Cl_2$ to increase water solubility. When a solution of $[\mathbf{3}]Cl_2$ in water was irradiated with a 445 nm LED, a change in the MLCT band of the UV-Vis spectra was observed, with a small bathochromic shift of the maximum absorption to 500 nm (**Figure 5c**). The steady state was reached after 60 min irradiation at the same photon flux as above ($\sim 3 \cdot 10^{-8}$ mol·s$^{-1}$). A mass spectrum of the irradiated sample showed no peaks that would correspond to the starting complex (**Figure S11**). When a solution of $[\mathbf{3}]Cl_2$ was kept in the dark and monitored with UV-Vis, a qualitatively similar but less pronounced change in the spectra was observed. When $[\mathbf{3}]Cl_2$ was dissolved in $D_2O$ to monitor the photoreaction with $^1$H NMR, two sets of peaks were present already at t = 0, with a doublet at 7.22 ppm (integrating for two H, characteristic of the $H_3$ position in the dmbpy), and two doublets at 7.30 and 7.35 ppm (integrating for one H each), indicating the presence of two species in a ratio of 1:0.5 (**Figure S8a**). When this mixture was kept in the dark at room temperature for 72 h, almost no change was observed. However, when the solution was irradiated with a Xe lamp mounted with a 450 nm bandpass filter, the doublets at 7.30 and 7.35 ppm disappeared after 3 hours, whereas the intensity of the doublet at 7.22 ppm increased (**Figure S8b**). This peak belongs to the solvated complex $[Ru(dmbpy)_2(OH_2)_2]^{2+}$. Thus, $[\mathbf{3}](PF_6)_2$ in water is not stable in the dark. The mtpa ligand is substituted by two water molecules, to reach an equilibrium between $[\mathbf{3}]^{2+}$ and $[Ru(dmbpy)_2(OH_2)_2]^{2+}$ (**Scheme 2**). In water this equilibrium can be displaced by light irradiation, as has been reported for other types of strained ruthenium complexes [11, 21].

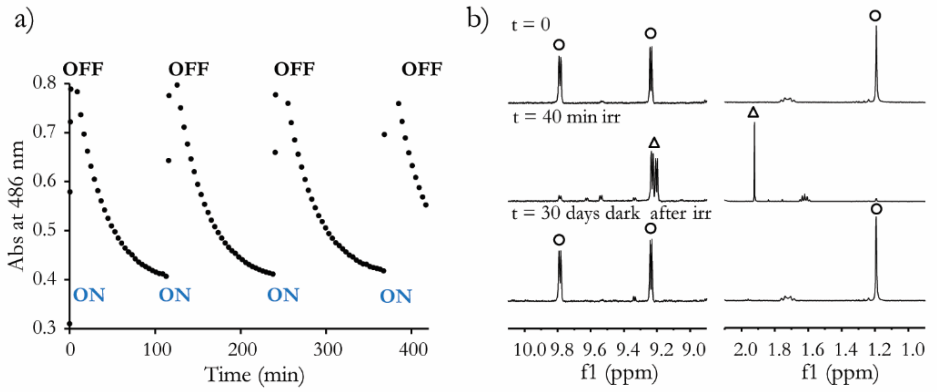


**Figure 6**. a) Evolution of the absorbance at 486 nm *vs.* time of a solution of $[\mathbf{1}](PF_6)_2$ in water (0.099 mM) upon switching ON and OFF several times a source of blue light ($\lambda_e$ = 445 nm, photon flux $2.9 \cdot 10^{-8}$ mol·s$^{-1}$) at 37 °C under $N_2$. b) Evolution of the $^1$H NMR spectra (regions 10 – 9 and 2 – 1 ppm) of a solution of $[\mathbf{1}](PF_6)_2$ in $D_2O$ (3.0 mM) irradiated with a Xe lamp for 40 min (ON) and then left in the dark for 30 days (OFF) at room temperature. The doublets at 9.79 and 9.24 ppm (circles) correspond to the $H_6$ protons on the bpy for complex $[\mathbf{1}]^{2+}$ and the arising doublets at 9.23 and 9.21 ppm (triangle) correspond to the $H_6$ proton on the bpy for the monodentate-bound mtpa ligand in $[Ru(bpy)_2(mtpa\text{-}\kappa N)(OH_2)]^{2+}$. The singlet at 1.20 ppm (circles) corresponds to the methyl thioether group, and the arising singlet at 1.92 ppm (triangle) corresponds to the decoordinated thioether.

Finally, the photoreactivity of the moderately strained complex $[\mathbf{2}](PF_6)_2$ was investigated by irradiating a solution of $[\mathbf{2}](PF_6)_2$ in water with a 445 nm LED. UV-Vis spectra showed a bathochromic shift of the absorption maximum from 464 nm to 492 nm, without any clear isosbestic point in the MLCT region (**Figure 5b**). Mass spectra after completion of the photoreaction showed peaks at m/z = 261.9 and 222.5, corresponding to $[Ru(dmbpy)(bpy)(CH_3CN)_2]^{2+}$ (calcd m/z = 262.1) and $[Ru(bpy)(mtpa)(CH_3CN)_2]^{2+}$ (calcd m/z = 222.5, **Figure S10**), which means that both dmbpy and mtpa ligands are photosubstituted in two parallel photoreactions. To confirm that photosubstitution of both mtpa and dmbpy occurred, white light irradiation of a solution of $[\mathbf{2}](PF_6)_2$ in $D_2O$ was monitored by $^1$H NMR. As shown in **Figure S7**, after 60 min the doublet of the starting complex at 9.57 ppm completely vanished, while three new doublets appeared in the 9.00 – 10.00 ppm range, at 9.72, 9.38, and 9.21 ppm in a 1:1:0.5 ratio. This result indicates that $[\mathbf{2}]^{2+}$ was fully converted into two new species, as the doublets at 9.72 and 9.38 ppm belong to the same species. In addition to these two new species, the signals of free dmbpy (7.86, 7.74, and 7.37 ppm)

and free mtpa (singlet at 2.10 ppm) were also found, thus confirming the competing photosubstitution of both dmbpy and mtpa. Although parallel photosubstitution of two distinct ligands has not been described very often, it has been observed recently in our group in a similar complex, [Ru(bpy)(dmbpy)(L-proline)]$PF_6$ [13].

These results highlight that methylated ligands are not always the ones that are photosubstituted, and that the selectivity of photosubstitution reactions is the result of a delicate interplay between the energies and shape of the triplet excited state hypersurface that is difficult to predict.

**Cytotoxicity assays**

The cytotoxicity of compounds [**1**]$(PF_6)_2$, [**2**]$(PF_6)_2$, [**3**]$(PF_6)_2$, and of the ligand mtpa was tested against A549 cancer cells (adenocarcinomic human alveolar basal epithelial cells) following a protocol detailed by Hopkins *et al* [22].

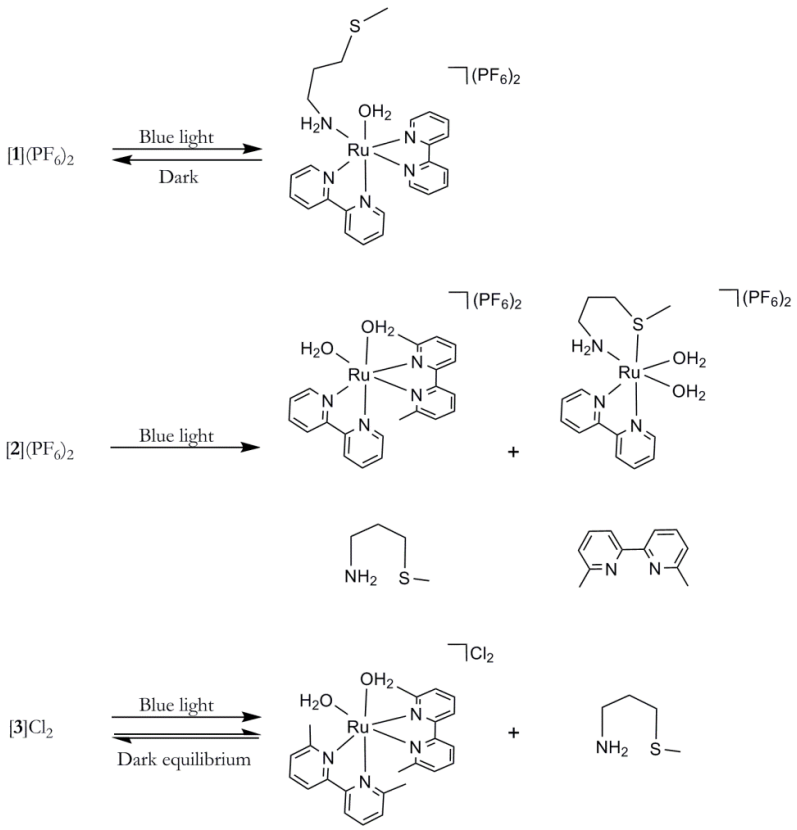


**Scheme 2**. Photoreaction and thermal equilibria in aqueous solutions of [**1**]$(PF_6)_2$, [**2**]$(PF_6)_2$, and [**3**]$Cl_2$.

We first verified that a light dose of 6.3 J·cm$^{-2}$ was *i)* enough to activate all three ruthenium compounds at the highest concentration used in the assays (86 μM, **Figure S12**), and *ii)* non-toxic to the A549 cell line [22]. The cells were irradiated with blue light (454 nm, dose of 6.3 J·cm$^{-2}$) 6 h after adding the compound, and further incubated for 48 h without refreshing the media. A sulforhodamine assay was performed at t = 96 h to compare the viability of treated *vs.* non-treated wells. The effective concentrations ($EC_{50}$), *i.e.* the compound concentration needed to decrease the cell survival to 50% compared to the non-treated control, was determined for each compound (**Table 2**). Importantly, the free ligand mtpa showed no significant cytotoxicity below 100 μM (**Figure S13**). Thus, unless the toxic ligand dmbpy is also released inside cells, all biological activities observed below

may be attributed to the metal-containing photoproduct [8]. As shown in **Figure 7a**, no significant toxicity was observed with [**1**](PF$_6$)$_2$, both in the dark and after blue light irradiation. On the other hand, [**3**](PF$_6$)$_2$ showed mild toxicity and similar EC$_{50}$ values in the dark and upon light activation (51.8 and 43.4 μM, respectively). In great contrast, [**2**](PF$_6$)$_2$ resulted in a large decrease of the EC$_{50}$ from 110 μM in the dark to 13.8 μM after light activation, corresponding to a photoindex (PI) of 8.

**Table 2**. (Photo)cytotoxicity (EC$_{50}$ with 95% Confidence Interval in μM) of [**1**](PF$_6$)$_2$, [**2**](PF$_6$)$_2$, [**3**](PF$_6$)$_2$, and mtpa on lung cancer cells (A549). Photoindices (PI) are defined as EC$_{50}$ dark/EC$_{50}$ light.

| | [1](PF$_6$)$_2$ | CI (95%) | [2](PF$_6$)$_2$ | CI (95%) | [3](PF$_6$)$_2$ | CI (95%) | mtpa | CI (95%) |
|---|---|---|---|---|---|---|---|---|
| **EC$_{50}$ dark (μM)** | >150 | - | 110 | +15 | 51.8 | +12.2 | >150 | - |
| | | - | | −13 | | −9.9 | | - |
| **EC$_{50}$ light (μM)** | >150 | - | 13.8 | +4.6 | 43.5 | +9.2 | >150 | - |
| | | - | | −3.4 | | −7.6 | | - |
| **PI** | - | | 8.0 | | 1.2 | | - | |

Overall, our data suggest that activation of the mtpa-based complexes via thermal- or light-induced substitution of one of the bidentate ligands by two water molecules is the key factor leading to cytotoxicity. According to spectroscopic studies, [**1**](PF$_6$)$_2$ is indeed not fully "activated" upon light irradiation, as only the thioether part of the mtpa ligand is substituted by one water molecule, without formation of the bis-aqua complex. This result, together with the probable low cellular uptake of complexes of that kind [8], may explain the absence of cytotoxicity after light activation.
On the other hand, [**3**](PF$_6$)$_2$ shows similar cytotoxicity in the dark and upon light irradiation because formation of the bis-aqua complex by substitution of mtpa occurs already in the dark. In other terms, it is too strained to be thermally stable, which prevents light activation by photosubstitution to be very efficient. However, a greater difference in EC$_{50}$ between dark and irradiated conditions may be expected because the thermal equilibrium between [**3**](PF$_6$)$_2$ and the bis-aqua complex is shifted towards the bis-aqua complex by light.

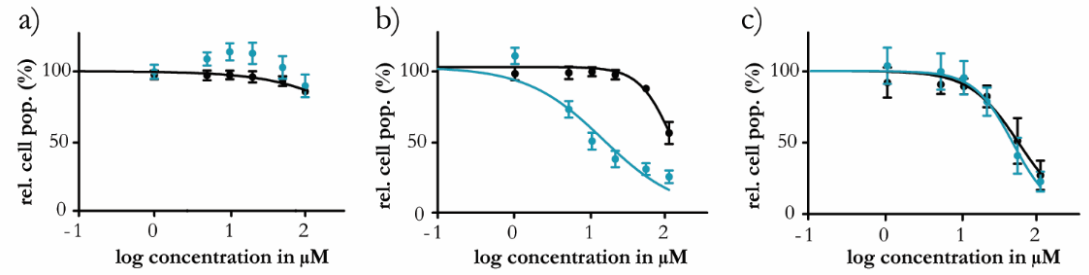


**Figure 7**. Dose-response curves for A549 cells in presence of a) [**1**](PF$_6$)$_2$, b) [**2**](PF$_6$)$_2$, or c) [**3**](PF$_6$)$_2$ irradiated with blue light (454 nm, 6.35 J·cm$^{-2}$) 6 h after treatment (blue data points) or left in the dark (black data points). Phototoxicity assay outline: cells seeded at 5·10$^3$ cells/well at t = 0 h, treated with [**1**](PF$_6$)$_2$, [**2**](PF$_6$)$_2$, or [**3**](PF$_6$)$_2$ at t =24 h, irradiated at t = 30 h, and SRB cell-counting assay performed at t = 96 h. Incubation conditions: 37 °C and 7.0% $CO_2$.

Considering the dynamics of speciation in a cell, the different modes by which the drug may be taken up, and the different localization of the prodrug and of the activated drug, it is difficult to claim that equilibrium shifts which are observed in a simple water solution can also occur in a cell and explain minute cytotoxicity differences between dark and irradiated conditions. On the other hand, it is clear that the compound with intermediate steric hindrance and intermediate lipophilicity, *i.e.* [**2**](PF$_6$)$_2$, shows at the same time a significant photoindex (8), a high thermal stability compared to [**3**](PF$_6$)$_2$, and a better photoreactivity

compared to [**1**]$(PF_6)_2$. This complex seems thus to be the optimal trade-off between stability and photoreactivity in this family of complexes.

## III. Conclusions

In this work, we have successfully synthesized a series of complexes bearing the non-toxic thioether mtpa ligand as caging ligand for a bis-aqua ruthenium polypyridyl species. As mtpa is a pro-chiral and dissymmetric bidentate ligand, many isomers are generated upon coordination to a ruthenium bis(diimine) complex. The challenging characterization of the geometries(s) effectively obtained was realized by a combination of X-ray crystallography, NOESY spectroscopy, and DFT calculations. While the non-strained complex $[\mathbf{1}]^{2+}$ is not capable of fully releasing mtpa and is poorly toxic to cancer cells, the more strained complexes $[\mathbf{2}]^{2+}$ and $[\mathbf{3}]^{2+}$ showed efficient mtpa photosubstitution upon blue light irradiation. In the mildly strained compound [**2**]$(PF_6)_2$ this leads to effective light activation of the compound toxicity in cancer cells. However, when fine-tuning steric hindrance and introducing two different "spectator" bipyridyl ligands as in $[\mathbf{2}]^{2+}$, we lost the selectivity of the photosubstitution reaction, as in $[\mathbf{2}]^{2+}$ both dmbpy and mtpa are substituted in parallel. The enhanced phototoxicity observed when $[\mathbf{2}]^{2+}$ is irradiated with light cannot be solely attributed to the photochemically generated *cis*-$[Ru(bpy)(dmbpy)(OH_2)_2]^{2+}$ species. The free dmbpy ligand, as demonstrated recently, is also toxic [8], and a second ruthenium-containing photoproduct, *cis*-$[Ru(bpy)(mtpa)(OH_2)_2]^{2+}$ is also released, the biological properties of which are unknown. Overall, adding methyl groups in hindering positions on the bipyridine ligands does allow for fine-tuning the lipophilicity and photoreactivity of light-activated ruthenium anticancer complexes. However, achieving selective substitution of a non-toxic ligand to study the biological properties of a single metal-based photoproduct remains a chemical challenge.

## IV. Additional Information

Supporting information is available online. Correspondence and requests for materials should be addressed to S.B.

## V. Materials and Methods

### Synthesis

**General**: The ligands 2,2'-bipyridine (bpy), 6,6'-dimethyl-2,2'-bipyridine (dmbpy), and 3-(methylthio)propylamine (mtpa) were purchased from Sigma-Aldrich, as well as cis-bis(2,2'-bipyridine)dichlororuthenium(II) hydrate (*cis*-$[Ru(bpy)_2Cl_2]$). Silver nitrate ($AgNO_3$) and potassium hexafluoridophosphate ($KPF_6$) were purchased from Alfa-Aesar. Triethylamine ($Et_3N$) was purchased from Merck. All reactants and solvents were used without further purification. The syntheses of cis-$[Ru(dmbpy)_2Cl_2]$, *rac*-$[Ru(bpy)(dmbpy)_2](PF_6)_2$ ([**5**]$(PF_6)_2$), and *rac*-$[Ru(bpy)(dmbpy)(MeCN)_2](PF_6)_2$ ([**4**]$(PF_6)_2$) were carried out according to literature procedures [13, 23]. Sephadex LH-20 was used for the Size Exclusion Column (SEC) chromatography. Electrospray mass spectra (ES MS) were recorded by using a Thermoquest Finnagen AQA Spectrometer and a MSQ Plus Spectrometer. All $^1H$ NMR spectra were recorded on a Bruker DPX-300 or DMX-400 spectrometers. Chemical shifts are indicated in ppm relative to the residual solvent peak. In the NOESY measurements, the mixing time was 1.0 s for complexes [**1**]$(PF_6)_2$ and [**3**]$(PF_6)_2$, and 0.5 s for complex [**2**]$(PF_6)_2$.

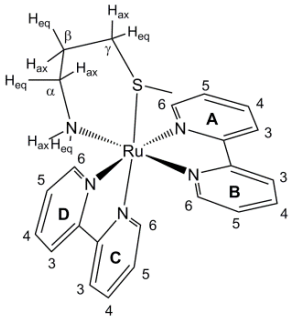

**[Ru(bpy)$_2$(mtpa)](PF$_6$)$_2$** ([**1**](PF$_6$)$_2$). *cis*-[Ru(bpy)$_2$Cl$_2$] (49 mg, 0.101 mmol) and $AgNO_3$ (36.5 mg, 0.214 mmol) were added to deaerated water (10 mL) and stirred under argon at 90 ºC for 30 min. After the solution was filtered to remove the grey solid formed (AgCl), $Et_3N$ (17 µL, 0.122 mmol) and mtpa (14 µL, 0.124 mmol) were added to the filtrate, which was stirred at 90 ºC for 1 hour under Ar. Then, after addition of a saturated $KPF_6$ aqueous solution, an orange precipitate was obtained. After filtration, the product was purified by SEC chromatography using $CH_3OH$ as eluent. The main orange fraction was collected and, after solvent evaporation, an orange solid was obtained. Yield: 40 mg (50%). Two isomers in a ratio 1:0.05. $^1$H NMR of the major isomer (Λ-(*S*), Δ-(*R*))-[**1**](PF$_6$)$_2$ (400 MHz, $D_2O$) δ 9.79 (d, J = 5.7 Hz, 1H, D6), 9.23 (d, J = 5.3 Hz, 1H, A6), 8.54 (t, J = 8.4 Hz, 2H, A3 + D3), 8.41 (d, J = 8.2 Hz, 1H, C3), 8.35 (d, J = 8.2 Hz, 1H, B3), 8.25 (t, J = 8.0 Hz, 1H, A4), 8.20 (td, J = 7.9, 1.5 Hz, 1H, D4), 7.93 (td, J = 7.9, 1.6 Hz, 1H, C4), 7.89 – 7.80 (m, 3H, A5 + B4 + D5), 7.65 (d, J = 5.5 Hz, 1H, B6), 7.56 (d, J = 5.6 Hz, 1H, C6), 7.25 (ddd, J = 7.2, 5.6, 1.4 Hz, 1H, C5), 7.14 (ddd, J = 7.2, 5.6, 1.4 Hz, 1H, B5), 3.92 (d, J = 12.1 Hz, 1H, $N_{eq}$), 3.17 – 2.92 (m, 3H, $\gamma_{eq}$ + $N_{ax}$ + $\alpha_{ax}$), 2.86 – 2.76 (m, 1H, $\alpha_{eq}$), 2.53 (t, J = 11.7 Hz, 1H, $\gamma_{ax}$), 2.28 – 2.15 (m, 1H, $\beta_{eq}$), 1.79 – 1.66 (m, 1H, $\beta_{ax}$), 1.19 (s, 3H, MeS-). Anal. Calcd for $C_{29}H_{32}F_6N_5O_2PRu$: C, 35.65; H, 3.37; N, 8.66 Found: C, 35.67; H, 3.34; N, 8.64. High Resolution ES MS m/z (calcd): 259.55127 (259.55098, $[1]^{2+}$), 664.06787 (664.0667, $[1 + PF_6]^+$).

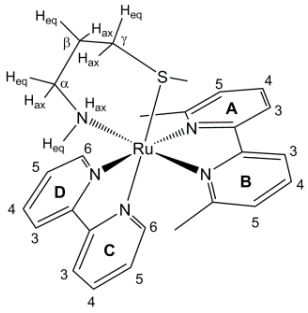

**[Ru(bpy)(dmbpy)(mtpa)](PF$_6$)$_2$** ([**2**](PF$_6$)$_2$). [**4**](PF$_6$)$_2$ (50 mg, 0.061 mmol), mtpa (13 µL, 0.120 mmol), and $Et_3N$ (45 µL, 0.322 mmol) were dissolved in deaerated water (5 mL) and refluxed under argon for 2 h, after which the solvent was removed under reduced pressure by rotary evaporation at 40 °C. The crude reaction mixture was purified by an alumina chromatography column using a DCM/$CH_3OH$ mixture in a gradient 0-1% of $CH_3OH$ as eluent. The yellow ($R_f$ = 0.65) and orange ($R_f$ = 0.6) fractions were collected and the solvent was removed under reduced pressure by rotary evaporation at 40 °C. Yield: 32 mg (62%). Two isomers in a ratio 1:0.09. $^1$H NMR of the the major isomer (Λ-(*R*), Δ-(S))-[**2a**](PF$_6$)$_2$ $^1$H NMR (400 MHz, $CD_3OD$) δ 9.55 (d, J = 5.4 Hz, 1H, D6), 8.71 (d, J = 7.8 Hz, 1H, D3), 8.65 (d, J = 8.1 Hz, 1H, C3), 8.45 (d, J = 7.8 Hz, 1H, A3), 8.29 (d, J = 7.9 Hz, 1H, B3), 8.25 (td, J = 7.9, 1.4 Hz, 1H, D4), 8.21 (d, J = 5.2 Hz, 1H, C6), 8.17 – 8.10 (m, 2H, A4 + C4), 7.86 – 7.80 (m, 2H, D5 + B4), 7.76 (dd, J = 7.8, 1.3 Hz, 1H, A5), 7.50 (ddd, J = 7.3, 5.7, 1.3 Hz, 1H, C5), 7.21 (dd, J = 7.8, 1.2 Hz, 1H, B5), 3.87 – 3.76 (m, 1H, $N_{ax}$), 3.14 – 3.01 (m, 2H, $N_{eq}$ + $\gamma_{ax}$ ), 2.92 (s, 3H, AMe), 2.67 – 2.57 (m, 1H, α), 2.53 – 2.43 (m, 1H, $\gamma_{eq}$), 2.17 – 2.07 (m, 1H, α), 2.06 – 1.97 (m, 1H, β), 1.96 – 1.87 (m, 1H, β), 1.62 (s, 3H, BMe), 1.58 (s, 3H, MeS-). $^{13}$C NMR (101 MHz, $CD_3OD$) δ 167.54, 167.01, 161.41, 161.35, 160.57, 159.71, 156.75, 155.03, 139.57, 139.28, 139.17, 138.75, 128.90, 128.39, 128.25, 127.87, 126.08, 125.46, 122.68, 122.46, 42.32, 35.25, 27.17, 26.48, 24.69, 17.74. Anal. Calcd for $C_{29}H_{32}F_6N_5O_2PRu$: C, 37.33; H, 3.73; N, 8.37 Found: C, 37.41; H,

3.87; N, 8.31. High Resolution ES MS m/z (calcd): 273.56708 (273.56663, $[2]^{2+}$), 692.09851 (692.09800, $[2 + PF_6]^+$).

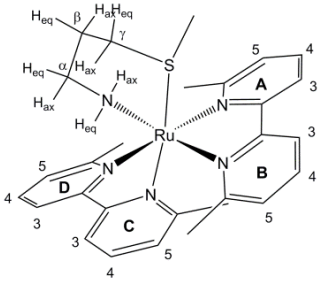


**[Ru(dmbpy)₂(mtpa)](PF₆)₂** ([**3**](PF₆)₂). *cis*-[Ru(dmbpy)₂Cl₂] (50.4 mg, 0.093 mmol) was dissolved in deaerated water (3 mL) and heated under argon at 60 °C for 5 min, after which mtpa (17 μL, 0.157 mmol) and $Et_3N$ (20 μL, 0.143 mmol) were added to the reaction mixture and stirred at 60 °C for 45 min. Then, after addition of saturated $KPF_6$ aqueous solution (1 mL), a reddish precipitate was obtained. The suspension was filtered and washed with cold water (5 mL) and diethyl ether. Yield: 40 mg (50%). Two isomers in a ratio 1:0.12. $^1$H NMR of the major isomer (Λ-(*S*), Δ-(*R*))-ax-[**3**](PF₆)₂ (400 MHz, $CD_3OD$) δ 8.53 (d, *J* = 7.9 Hz, 1H, D3), 8.50 (d, *J* = 8.2 Hz, 1H, C3), 8.44 (t, *J* = 8.6 Hz, 2H, A3 + B3), 8.12 (td, *J* = 7.9, 3.4 Hz, 1H, D4 + A4), 8.06 (t, *J* = 7.9 Hz, 1H, C4), 7.97 (t, *J* = 7.9 Hz, 1H, B4), 7.68 (td, *J* = 7.5, 1.3 Hz, 2H, A5 + D5), 7.45 (d, *J* = 7.8 Hz, 1H, C5), 7.41 (d, *J* = 7.8 Hz, 1H, B5), 3.26 – 3.18 (m, 1H), 2.83 (s, 3H, DMe), 2.75 – 2.68 (m, 1H, $\gamma_{eq}$), 2.67 (s, 3H, AMe), 2.50 (d, *J* = 12.6 Hz, 1H), 2.44 – 2.33 (m, 1H, $\gamma_{ax}$), 1.94 (s, 3H, BMe), 1.86 (s, 3H, CMe), 1.79 – 1.68 (m, 1H), 1.20 (s, 3H, MeS-), 0.33 (d, *J* = 12.0 Hz, 1H). $^{13}$C NMR (101 MHz, acetone-d6) δ 168.21, 167.82, 167.35, 167.27, 161.13, 160.95, 160.34, 160.14, 139.16, 139.03, 138.91, 138.28, 128.15, 127.45, 127.32, 126.93, 124.33, 123.34, 123.04, 122.43, 41.93, 34.74, 26.39, 25.35, 24.60, 24.39, 23.38, 15.62. Anal. Calcd for $C_{29}H_{32}F_6N_5O_2PRu$: C, 38.89; H, 4.08; N, 8.10 Found: C, 38.02; H, 4.18; N, 7.64. High Resolution ES MS m/z (calcd): 287.58243 (287.58228, $[3]^{2+}$), 720.12781 (720.12930, $[3 + PF_6]^+$).

## Photochemistry

**General**: For the irradiation experiments of NMR tubes, the light of a LOT 1000 W Xenon Arc lamp mounted with infrared and 400 nm long pass filters was used. When specified, a 450 nm 450FS10-50 filter from Andover Corporation filter was used. For NMR experiments under $N_2$, NMR tubes with PTFE stopper were used. UV-Vis experiments were performed on a Cary 50 Varian spectrometer. When monitoring photoreactions with UV-Vis and mass spectrometry, a LED light source ($\lambda_{ex}$ = 445 nm, with a Full Width at Half Maximum of 14 nm, Part. No H2A1-H450, Roithner LaserTechnik, Vienna, Austria) with a photon flux between $2.79 \cdot 10^{-8}$ and $2.98 \cdot 10^{-8}$ mol·s$^{-1}$ was used.

**Experiments monitored with $^1$H NMR**: A stock solution in deuterated water of either [**1**](PF₆)₂, [**2**](PF₆)₂, or [**3**]$Cl_2$ was prepared and deaerated under $N_2$ (see **Table 3** for the details). Then, 600 μL of the stock solution were transferred, under $N_2$, into a NMR tube. The tube was irradiated at room temperature with a LOT Xenon 1000 W lamp equipped with an IR short pass and a >400 nm long pass filters. In addition, a control experiment without white light irradiation was performed. The reactions were monitored with $^1$H NMR at various time intervals.

**Table 3**. Conditions of the photoreactions of [**1**](PF$_6$)$_2$, [**2**](PF$_6$)$_2$, and [**3**]Cl$_2$ in D$_2$O monitored with $^1$H NMR.

| Complex | w (mg) | V (µL) | $M_w$ (g/mol) | Concentration (mM) |
|---|---|---|---|---|
| **[1](PF$_6$)$_2$** | 1.6 | 660 | 808.57 | 3.0 |
| **[2](PF$_6$)$_2$** | 1.0 | 600 | 836.63 | 2.0 |
| **[3]Cl$_2$**[a] | 1.0 | 600 | 645.65 | 2.6 |

[a] Complex [3](PF$_6$)$_2$ was converted to [3]Cl$_2$ for solubility reasons, by addition of Bu$_4$NCl in acetone, followed by filtration and washing with cold acetone and diethyl ether.

**Irradiation experiments monitored with UV-Vis and MS**: UV-Vis spectroscopy was performed using a UV-Vis spectrometer equipped with temperature control set to 25 or 37 °C and a magnetic stirrer. The irradiation experiments were performed in a quartz cuvette containing 3 mL of solution. A stock solution of the desired complex was prepared using demineralized water, which was then diluted in the cuvette to a working solution concentration. When the experiment was carried out under $N_2$ the sample was deaerated for 15 min by gentle bubbling of $N_2$ and the atmosphere was kept inert during the experiment by a gentle flow of $N_2$ on top of the cuvette. A UV-Vis spectrum was measured every 30 s for the first 10 min, every 1 min for the next 10 min, and eventually every 10 min until the end of the experiment. Data was analysed with Microsoft Excel. Experimental conditions are detailed in **Table 4**.

**Table 4**. Conditions of the photoreactions of [**1**](PF$_6$)$_2$, [**2**](PF$_6$)$_2$, and [**3**]Cl$_2$ in demineralized water monitored with MS and UV-Vis.

| Complex | Stock solution | | | | Working solution (mM) | Photonflux 445 nm LED (mol·s$^{-1}$) | Temperature (°C) |
|---|---|---|---|---|---|---|---|
| | w (mg) | V (mL) | $M_w$ (g/mol) | M (mM) | | | |
| **[1](PF$_6$)$_2$** | 2.4 | 10 | 808.57 | 0.297 | 0.145 | $2.95\cdot10^{-8}$ | 25 |
| | | | | | 0.099 | $2.91\cdot10^{-8}$ | 37 |
| **[2](PF$_6$)$_2$** | 0.63 | 5 | 836.63 | 0.151 | 0.101 | $2.92\cdot10^{-8}$ | 25 |
| **[3]Cl$_2$**[a] | 1.58 | 10 | 645.65 | 0.245 | 0.123 | $2.79\cdot10^{-8}$ | 25 |

[a] Complex [3](PF$_6$)$_2$ was converted to [3]Cl$_2$ for solubility reasons, by addition of Bu$_4$NCl in acetone, followed by filtration and washing with cold acetone and diethyl ether.

**Blue light irradiation in the cell irradiation setup**: The photochemical reactivity of [**1**](PF$_6$)$_2$, [**2**](PF$_6$)$_2$, and [**3**](PF$_6$)$_2$ in 96-well plates was measured using UV-Vis spectroscopy. Solutions of each compound were prepared in Opti-MEM complete (86 µM), transferred into a 96-well plate, and irradiated with blue light (454 nm) at different irradiation times using the blue LED source described in details in Hopkins *et al.* to mimic the conditions used in the photocytotoxicity assay [22]. **Figure S12** shows that the three complexes are fully activated at 86 µM after 10 minutes irradiation. Thus, 10 minutes was chosen as the blue light irradiation time in the photocytotoxity assay, which corresponded to a dose of 6.3 J.cm$^{-2}$.

## Crystal growing and X-ray structure

**General**: All reflection intensities were measured at 110(2) K using a SuperNova diffractometer (equipped with Atlas detector) with Cu *K*α radiation (λ = 1.54178 Å) or Mo *K*α radiation (λ = 0.71073 Å) under the program CrysAlisPro (Version 1.171.36.32 Agilent Technologies, 2013). The same program was used to refine the cell dimensions and for data reduction. The structure was solved with the program SHELXS-2013 and was refined on $F^2$ with SHELXL-2013 [24]. Analytical numeric absorption correction based on a multifaceted crystal model was applied using CrysAlisPro. The temperature of the data collection was controlled using the system Cryojet (manufactured by Oxford Instruments). The H atoms were placed at calculated positions (unless otherwise specified) using the instructions AFIX 23, AFIX 43, AFIX 137 or AFIX 147 with isotropic displacement parameters having values 1.2 *U*eq of the attached C or O atoms.

**Complex [1](PF$_6$)$_2$·CH$_3$OH**

**Crystal growth**: [**1**](PF$_6$)$_2$ (1.0 mg) was dissolved in CH$_3$OH (1 mL, 1.2 mM) in a GC vial, which was placed in a larger vial that contained toluene (3 mL) as a counter solvent. The large vial was stoppered. After a few days X-ray quality crystals were obtained by vapour diffusion.

**Crystal structure determination**: The H atoms attached to N5 were found from difference Fourier maps, and their coordinates and isotropic temperature factors were refined freely.

**Details of the crystal structure**: The structure is mostly ordered. The lattice CH$_3$OH solvent molecule is disordered over two orientations and the occupancy factor of the major component of the disorder refines to 0.70(2). Fw = 840.62, red block, 0.38 × 0.28 × 0.25 mm$^3$, monoclinic, *C*2/*c* (no. 15), *a* = 12.5589(2), *b* = 14.0651(2), *c* = 36.3739(7), $\beta$ = 98.5152(18)°, *V* = 6354.34(19) Å$^3$, *Z* = 8, $D_x$ = 1.757 g cm$^{-3}$, $\mu$ = 6.502 mm$^{-1}$, $T_{min}$–$T_{max}$: 0.224–0.383. 20578 Reflections were measured up to a resolution of (sin $\theta/\lambda)_{max}$ = 0.62 Å$^{-1}$. 6232 Reflections were unique ($R_{int}$ = 0.0175), of which 6168 were observed [$I > 2\sigma(I)$]. 449 Parameters were refined using 37 restraints. *R*1/*w*R2 [$I > 2\sigma(I)$]: 0.0335/0.0811. *R*1/*w*R2 [all refl.]: 0.0339/0.0814. S = 1.147. Residual electron density found between −0.68 and 0.84 e Å$^{-3}$.

**Complex [2a](PF$_6$)$_2$**

**Crystal growth**: [**2**](PF$_6$)$_2$ (1.0 mg) was dissolved in CH$_3$OH (1 mL, 1.2 mM) in a GC vial, which was placed in a larger vial that contained ethyl acetate (3 mL) as a counter solvent. The large vial was stoppered. After few days X-ray quality crystals were obtained by vapour diffusion.

**Crystal structure determination**: The H atoms attached to N5 were found from difference Fourier map, and their coordinates and isotropic temperature factors were refined freely. The structure is partly disordered.

**Details of the crystal structure**: One of the two $PF_6^-$ counter ions is disordered over 3 orientations. The occupancy factors of the three different orientation can be retrieved in the .cif file. Fw = 836.63, 0.24 × 0.21 × 0.07 mm$^3$, orthorhombic, Pbca, *a* = 9.17330(14), *b* = 18.2183(3), *c* = 36.9112(5), *V* = 6168.67(16) Å$^3$, *Z* = 8, $\mu$ = 6.67 mm$^{-1}$, $T_{min}$–$T_{max}$: 0.331–0.673. 36039 Reflections were measured up to a resolution of (sin $\theta/\lambda)_{max}$ = 0.616 Å$^{-1}$. 6052 Reflections were unique ($R_{int}$ = 0.039), of which 5360 were observed [$I > 2\sigma(I)$]. 552 Parameters were refined using 619 restraints. $R[F^2 > 2\sigma(F^2)]$: 0.028. $wR(F^2)$: 0.067. S = 1.04. Residual electron density found between −0.58 and 0.56 e Å$^{-3}$.

**Complex [3](PF$_6$)$_2$**

**Crystal growth**: [**3**](PF$_6$)$_2$ (1.0 mg) was dissolved in CH$_3$OH (1 mL, 1.2 mM) in a GC vial, which was placed in a larger vial that contained di-*tert*-butyl ether (3 mL) as a counter solvent. The large vial was stoppered. After few days X-ray quality crystals were obtained by vapour diffusion.

**Crystal structure determination**: The structure is partly disordered.

**Details of the crystal structure**: One of the two $PF_6^-$ counterions is found to be disordered over three orientations, and the occupancy factors of the three components refine to 0.732(3), 0.180(3) and 0.088(3). Fw = 864.68, 0.21 × 0.16 × 0.05 mm$^3$, triclinic, P-1, *a* = 10.6739(3), *b* = 11.7852(3), *c* = 14.2773(4), *V* = 1662.91(8) Å$^3$, *Z* = 2, $\mu$ = 0.73 mm$^{-1}$, $T_{min}$–$T_{max}$: 0.661–1.000. 25022 Reflections were measured up to a resolution of (sin $\theta/\lambda)_{max}$ = 0.650 Å$^{-1}$. 7639 Reflections were unique ($R_{int}$ = 0.038), of which 6580 were

observed [$I > 2\sigma(I)$]. 564 Parameters were refined using 253 restraints. $R[F^2 > 2\sigma(F^2)]$: 0.035. $wR(F^2)$: 0.078. S = 1.03. Residual electron density found between −0.52 and 1.14 e Å$^{-3}$.

## DFT calculations

Electronic structure calculations were performed using DFT as implemented in the ADF program (SCM). The structures of all possible isomers of [**1**]$^{2+}$, [**2a**]$^{2+}$, [**2b**]$^{2+}$, and [**3**]$^{2+}$ were optimized in water using the conductor-like screening model (COSMO) to simulate the effect of solvent. The PBE0 [31] functional and a triple zeta potential basis set (TZP) were used for all calculations.

## Cell culture and $EC_{50}$ (photo)cytotoxicity assay

### General:

Human cancer cell line A549 (human lung carcinoma) was distributed by the European Collection of Cell Cultures (ECACC), and purchased from Sigma Aldrich. Dulbecco's Modified Eagle Medium (DMEM, with and without phenol red, without glutamine), Glutamine-S (GM; 200 mm), trichloroacetic acid (TCA), glacial acetic acid, sulfo-rhodamine B (SRB), and tris(hydroxylmethyl)aminomethane (Trisbase) were purchased from Sigma Aldrich. Fetal calf serum (FCS) was purchased from Hyclone. Penicillin and streptomycin were purchased from Duchefa and were diluted to a 100 mg/mL penicillin/streptomycin solution (P/S). Trypsin and Opti-MEM (without phenol red) were purchased from Gibco Life Technologies. Trypan blue (0.4% in 0.81% sodium chloride and 0.06% potassium phosphate dibasic solution) was purchased from BioRad. Plastic disposable flasks and 96-well plates were purchased from Sarstedt. Cells were counted by using a BioRad TC10 automated cell counter with Biorad cell-counting slides. UV-Vis measurements for analysis of 96-well plates were performed with a M1000 Tecan Reader. Cells were inspected with an Olympus IX81 microscope.

### Cell culture

Cells were cultured in Dulbecco's Modified Eagle Medium containing phenol red, supplemented with 8.0% v/v fetal calf serum (FCS), 0.2% v/v penicillin/streptomycin and 0.9% v/v glutamax. Cells were incubated at 37 ºC at 7.0% $CO_2$ in 75 cm² T-flask and split once a week at 80-90% confluency. Cells were cultured for a maxium of 8 weeks for all biological experiments, and passaged at least twice after being thawed.

### Cell-irradiation setup

The cell-irradiation system consisted of a Ditabis thermostat (980923001) fitted with two flat-bottomed micro-plate thermoblocks (800010600) and a 96-LED array fitted to a standard 96-well plate. The 454 nm LED (OVL-3324), 520 nm LED (OVL-3324), fans (40 mm, 24 VDC, 9714839), and power supply (EA-PS 2042-06B) were obtained from Farnell. See Hopkins *et al.* for a full description [22].

### Cytotoxicity assays

A549 cells were seeded at t = 0 in 96-well plates at a density of 5000 cells/well in Opti-MEM supplemented with 2.4% v/v FCS, 0.2% v/v P/S, and 1.0% v/v glutamax (called Opti-MEM complete) (100 µL) and incubated for 24 h at 37 ºC and 7.0% $CO_2$. After this period, aliquots (100 µL) of six different concentrations (1–100 µM for all the compounds) of freshly prepared stock solutions of [**1**]$(PF_6)_2$, [**2**]$(PF_6)_2$, [**3**]$(PF_6)_2$, and mtpa in Opti-MEM were added to the wells in triplicate. Sterilized dimethylsulfoxide (DMSO) was used to dissolve the compounds in such amounts that the maximum v/v% of DMSO per well did not exceed 0.5% v/v%. For every irradiated plate a parallel control plate was prepared and treated identically to the irradiated plate, but without irradiation. Plates were incubated in the dark for 6 h. After this period, half of the plates were irradiated and the other half were kept in the dark. After irradiation all

the plates were incubated in the dark until time 96 h after seeding. The cells were fixated by adding cold TCA (10 % w/v; 100 µL) in each well and the plates were stored at 4 °C for at least 4 h as part of the sulforhodamine B (SRB) assay that was adapted from Vichai *et al* [25]. In short, after fixation, the TCA mixture was removed from the wells, rinsed with demineralized water three times and air dried. Then, each well was stained with 100 µL SRB (0.6% w/v in 1% v/v acetic acid) for 30 min. The SRB was removed by washing with acetic acid (1 % v/v), and air dried. The SRB dye was solubilized with Tris base (10 mM; 200 µL), and the absorbance in each well was read at λ = 510 nm by using a M1000Tecan Reader.

The SRB absorbance data per compound per concentration was averaged over three identical wells (technical replicates, $n_t$ = 3) in Excel and made suitable for use in GraphPad Prism. Relative cell populations were calculated by dividing the average absorbance of the treated wells by the average absorbance of the untreated wells. In any case, it was checked that the cell viability of the untreated cells of the samples irradiated were similar (maximum difference of 10%) to the non-irradiated samples to make sure no harm was done by light alone. The data from three independent biological replications was plotted versus log (concentration in µM). The resulting dose-response curve for each compound under dark and irradiated conditions was fitted to a non-linear regression function with fixed *y* maximum (100%) and minimum (0%) (relative cell viability) and a variable Hill slope, to obtain the effective concentration ($EC_{50}$ in µM). The simplified two-parameter Hill-slope equation used for the fitting is shown in Equation 1:

$$\frac{100}{\left(1+10^{\left((\log_{10}EC50-X)\cdot Hill\ slope\right)}\right)}$$

**Equation 1**

Photo indices (PI) reported in **Table 2** were calculated, for each compound, by dividing the $EC_{50}$ value obtained in the dark by the $EC_{50}$ value determined under light irradiation.

## VI. Conflict of Interests

The authors declare there are no conflict of interests.

## VII. Acknowledgements

The European Research Council is acknowledged for a Starting grant to S.B. The Netherlands Organization for Scientific Research (NWO-CW) is acknowledged for a VIDI grant to S.B. Dr. Bianka Siewert, Dr. Samantha L. Hopkins and Prof. Elisabeth Bouwman are acknowledged for scientific discussion and support.

## VIII. References

[1] Shi G., Monro S., Hennigar R., Colpitts J., Fong J., Kasimova K., Yin H., DeCoste R., Spencer C., Chamberlain L., Mandel A., Lilge L., McFarland S. A., *Coord. Chem. Rev.* **2015**, *282–283*, 127-138.

[2] Huang H., Yu B., Zhang P., Huang J., Chen Y., Gasser G., Ji L., Chao H., *Angew. Chem. Int. Ed.* **2015**, *54*, 14049-14052.

[3] Pierroz V., Rubbiani R., Gentili C., Patra M., Mari C., Gasser G., Ferrari S., *Chem. Sci.* **2016**, *7*, 6115-6124.

[4] Wachter E., Heidary D. K., Howerton B. S., Parkin S., Glazer E. C., *Chem. Commun.* **2012**, *48*, 9649-9651.

[5] Garner R. N., Gallucci J. C., Dunbar K. R., Turro C., *Inorg. Chem.* **2011**, *50*, 9213-9215.

[6] Howerton B. S., Heidary D. K., Glazer E. C., *J. Am. Chem. Soc.* **2012**, *134*, 8324-8327.

[7] Sainuddin T., Pinto M., Yin H., Hetu M., Colpitts J., McFarland S. A., *J. Inorg. Biochem.* **2016**, *158*, 45-54.

[8] Cuello-Garibo J. A., Meijer M. S., Bonnet S., *Chem. Commun.* **2017**, *53*, 6768-6771.

[9] Azar D. F., Audi H., Farhat S., El-Sibai M., Abi-Habib R. J., Khnayzer R. S., *Dalton. Trans.* **2017**, *46*, 11529-11532.

[10] Goldbach R. E., Rodriguez-Garcia I., van Lenthe J. H., Siegler M. A., Bonnet S., *Chem. Eur. J.* **2011**, *17*, 9924-9929.

[11] Bahreman A., Limburg B., Siegler M. A., Bouwman E., Bonnet S., *Inorg. Chem.* **2013**, *52*, 9456-9469.

[12] Respondek T., Garner R. N., Herroon M. K., Podgorski I., Turro C., Kodanko J. J., *J Am Chem Soc.* **2011**, *133*, 17164-17167.

[13] Cuello-Garibo J.-A., Pérez-Gallent E., van der Boon L., Siegler M. A., Bonnet S., *Inorg. Chem.* **2017**, *56*, 4818-4828.

[14] Fleet M. E., *Mineral. Mag.* **1976**, *40*, 531-533.

[15] Dikhtiarenko A., Villanueva-Delgado P., Valiente R., García J., Gimeno J., *Polymers* **2016**, *8*, 48.

[16] van Rixel V. H. S., Siewert B., Hopkins S. L., Askes S. H. C., Busemann A., Siegler M. A., Bonnet S., *Chem. Sci.* **2016**, *7*, 4922-4929.

[17] Filevich O., Salierno M., Etchenique R., *J. Inorg. Biochem.* **2010**, *104*, 1248-1251.

[18] Arakawa R., Tachiyashiki S., Matsuo T., *Anal. Chem.* **1995**, *67*, 4133-4138.

[19] Zayat L., Filevich O., Baraldo L. M., Etchenique R., *Philos. Trans. R. Soc. London, A* **2013**, *371*, 20120330.

[20] Tachiyashiki S., Mizumachi K., *Coord. Chem. Rev.* **1994**, *132*, 113-120.

[21] Bahreman A., Limburg B., Siegler M. A., Koning R., Koster A. J., Bonnet S., *Chem. Eur. J.* **2012**, *18*, 10271-10280.

[22] Hopkins S. L., Siewert B., Askes S. H. C., Veldhuizen P., Zwier R., Heger M., Bonnet S., *Photochem. Photobiol. Sci.* **2016**, *15*, 644-653.

[23] Collin J. P., Sauvage J. P., *Inorg. Chem.* **1986**, *25*, 135-141.

[24] Sheldrick G. M., *Acta Crystallogr. Sect. A: Found. Adv.* **2008**, *64*, 112-122.

[25] Vichai V., Kirtikara K., *Nat. Protocols* **2006**, *1*, 1112-1116.

Received: 08 October 2017
Accepted: 13 November 2017
Published online: 01 December 2017

ORCID ID for authors
Sylvestre Bonnet: 0000-0002-5810-3657
Jordi-Amat Cuello-Garibo: 0000-0003-2375-2857